

VIII- II -1. Project Research

Project 11

Y. Saito

Research Reactor Institute, Kyoto University

1. Objectives and Allotted Research Subjects

Neutron imaging provides valuable information which cannot be obtained from an optical or X-ray imaging. The purpose of this project is to develop the imaging method itself and also the experimental environment for expanding the application area of the neutron imaging. The allotted research subjects are as follows:

- ARS-1 Measurements of Multiphase Dynamics by Neutron Radiography (Y. Saito *et al.*)
- ARS-2 Visualization and Measurement of Adsorption/Desorption Process of Ethanol in Activated Carbon Adsorber for Adsorption Heat Pump (N. Takenaka *et al.*)
- ARS-3 Neutron Radiography on Tubular Flow Reactor for Supercritical Hydrothermal Synthesis of Nanoparticles (T. Tsukada *et al.*)
- ARS-4 Characteristics of the Void Fraction under Transient Condition (H. Umekawa *et al.*)
- ARS-5 Neutron imaging and optics development using simulation of VCAD Systems (Y. Yamagata *et al.*)
- ARS-6 Water and Salt Distribution in a Rice Hull Medium under Sodium Chloride Solution Culture (U. Matsushima *et al.*)
- ARS-7 Measurement of Water Content in Hardened Cement Paste by Neutron Imaging (T. Numao *et al.*)
- ARS-8 Hydrazine Thickness Measurement by Neutron Radiography at a Catalyst Bed during Operation (H. Kagawa *et al.*)
- ARS-9 Development of Neutron Imaging Devices (H. Iikura *et al.*)
- ARS-10 In-situ Neutron Radiography Investigation on the Hydraulic Behavior of High Strength Cement Paste under High Temperature (M. Kanematsu *et al.*)
- ARS-11 Evaluation of coolant distribution in a flat heat-pipe type heat spreader (K. Mizuta *et al.*)

2. Main results and the contents of this report

In ARS-1, simultaneous measurements of water film distribution in an air-water two-phase flow were performed by using an electrical conductance method and high frame rate neutron radiography to complement their shortcomings in spatial or temporal resolutions.

ARS-2 applied neutron radiography to heat transfer study on an adsorption refrigerator. In this ARS, visualization of adsorption amount distributions of ethanol in an activated carbon powder bed. Experimental results show

that transient behaviors of adsorption amount distribution could be clearly observed by neutron radiography.

ARS-3 visualized the flow in a tubular flow reactor for supercritical hydrothermal synthesis using neutron radiography. It was demonstrated that neutron imaging with CT technique can visualize the 3D distributions of water density in a tubular flow reactor.

In ARS-4, the void fraction fluctuation was investigated under several forced convective flow boiling conditions. Especially, the influence of the heat capacity of the tube was clarified in this ARS.

ARS-5 conducted neutron radiography experiments at KUR E-2 port for 3D image reconstruction using VCAD system as well as neutron focusing mirror development. Visualization of glue between steel plates and Neutron Optics reflectometry test were performed.

ARS-6 investigated the relationship between the plant root system and water movement in a rice hull medium. The changes in water and salt distribution in a root system were investigated in rice hull medium under static solution culture.

ARS-7 evaluated the water distribution in the hardened cement paste (HPC) using neutron radiography. In this study, experiments were carried out to investigate a beam-hardening effect while neutron beam penetrating the HPC to quantify the moisture content in HPC.

ARS-8 applied neutron imaging to observation of a thruster, which is one of the key sub-components for spacecraft using fluids as propellants at the B4-port. In this subject, dynamic behavior of hydrazine in the thruster was observed by high frame rate neutron imaging. Results show periodic brightness fluctuations in the images corresponding the actual hydrazine behavior in the thruster.

ARS-9 investigated the influence of the thickness and prism pitch of brightness enhancement films (BEFs) on the brightness and spatial resolution of a neutron imaging system.

ARS-10 applied neutron radiography to detect the hydraulic behavior under high temperatures to understand the spalling phenomenon of high strength concrete.

ARS-11 applied neutron radiography to observe coolant distributions in a flat heat spreader (FGHP). Results indicate that uniform coolant distribution in FGHP can be realized regardless of the heat input and installation posture, which may lead the uniform heat spreading performance of FGHP under its operating conditions.

PR11-1 Visualization of Two-Phase Flow Dynamics by Neutron Radiography

Y. Saito, D. Ito and Y. Kawabata

Research Reactor Institute, Kyoto University

INTRODUCTION: Neutron radiography is a powerful tool for fluid flow visualization as well as multiphase flow research. Multiphase flows in a metallic pipe have been visualized clearly by using neutron radiography (NRG). However, it would be still difficult to obtain dynamic information on such multiphase flows by NRG, because of insufficient neutron flux from neutron sources and poor efficiency of imaging devices. In this work, our imaging system was improved for high frame rate NRG. Then, the system was applied to air-water two-phase flow measurements in a narrow rectangular channel. In addition, simultaneous measurements with an electrical conductance method, which has higher temporal resolution up to 10,000 Hz, was carried out to investigate the interfacial structure of the two-phase flow.

EXPERIMENTS: Experiments were performed at the B-4 supermirror neutron guide facility [1] of the Kyoto University Research Reactor Institute. The neutron flux of the B-4 port is 5×10^7 n/cm²s and the beam size is 10×75 mm² at the beam exit. An imaging system for high frame rate NRG consists of a neutron converter (⁶LiF/ZnS(Ag)), a dark box with a single mirror, a megapixel lens (VF50095M, SPACECOM), an image intensifier (single MCP (GaAsP) + Booster, Hamamatsu Photonics K.K.) and a high speed camera (MotionPro Y4 Lite, IDT Co. Ltd.), as shown in Fig.1. Since the measured images include severe signal noises due to the statistical error in counting neutrons, a spatio-temporal image filter was applied to enhance the quality of the images. Finally, the NRG images were used to estimate the void fraction in the channel gap with Σ -scaling method [2].

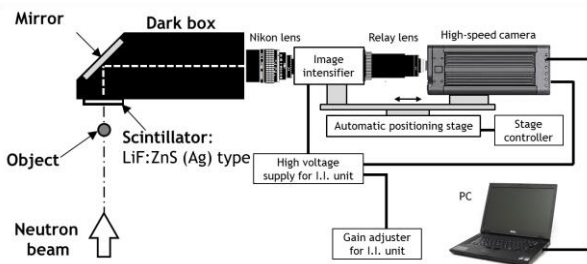


Fig. 1. Imaging system for high frame rate neutron radiography

The test section has a rectangular cross section with 12 mm width and 2 mm gap. The vertical channel was placed at 1m away from the neutron beam exit. The test fluids are air and tap water at room temperature. A liquid

film sensor (LFS) [3] based on an electrical conductance measurement was applied to visualize the water film flowing in the narrow channel, which was installed on one side of the channel walls. LFS has 7×32 measurement points and the distance between the points was 1.5 mm. The temporal resolutions of both measurements were 200 Hz for NRG and 10,000 Hz for LFS.

RESULTS: The typical results obtained by a simultaneous measurement with NRG and LFS were shown in Fig.2. This figure represents the instantaneous distributions at the same instant. Spatial distribution of void fraction was obtained from NRG image and the distribution of the water film thickness between the bubble and the wall was measured by LFS. From this result, NRG could visualize the bubble shape clearly, however it was difficult to detect the water film thickness less than hundreds μ m because of the image noises. In contrast, though LFS has less measurement points, it could measure thin film thickness at higher frame rate. Thus, the combination of two different methods with different resolutions might lead to further understanding of detailed structure in gas-liquid two-phase flows.

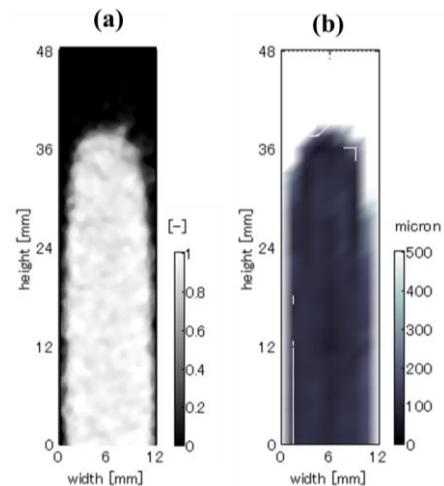


Fig. 2. Typical result of simultaneous measurement; (a) void fraction measured by NRG, (b) film thickness measured by LFS

REFERENCES:

- [1] Y. Saito, *et al.*, Nucl. Instr. Meth. Phys. Res., A, **651** (2011) 36-41.
- [2] K. Mishima and T. Hibiki, Nucl. Eng. Design, **184** (1998) 183-201.
- [3] M. Damsohn and H.-M. Prasser, Flow Meas. Instrum., **20** (2009) 1-14.

PR11-2 Visualization and Measurement of Adsorption/Desorption Process of Ethanol in Activated Carbon Adsorber for Adsorption Heat Pump

H. Asano, N. Takenaka, H. Murata, K. Sugimoto,
K. Murata, Y. Kawabata¹, Y. Saito¹ and D. Ito¹

Department of Mechanical Engineering, Kobe University
¹Research Reactor Institute, Kyoto University

INTRODUCTION: Adsorption refrigerator is one of the efficient tools to recover waste heat at a low temperature. A design of the adsorber, in which refrigerant is adsorbed in adsorbent particle bed, is a key part for the performance improvement. It is important to optimize the configuration to minimize the amount of driving heat, and to clarify adsorption/desorption phenomena in transient conditions. Neutron radiography was applied to visualize the adsorption amount distribution of ethanol in a activated carbon powder bed. The effect of fin arrangement for the enhancement of heat diffusion was considered.

EXPERIMENTS: Activated carbon and ethanol was used as the adsorbent and refrigerant, respectively. Activated carbon was packed in a aluminum frame shown in Fig. 1. The container was connected to an ethanol reservoir. The vapor pressure in the container could be maintained by the temperature of the reservoir. The front and back walls were made of thin SUS plates to avoid heat diffusion through these walls. The adsorber should be cooled in adsorption process or heated in desorption process by water through a channel in the bottom wall. Temperatures at the bottom of the adsorbent bed and three points in the bed as shown in Fig. 1 were measured by the inserted thermocouples. Two aluminum fins were placed in the adsorbent bed to enhance the heat diffusion. The adsorbent bed in transient processes was visualized by neutron radiography.

RESULTS: Examples of obtained images are shown in Fig. 2. Exposure time and pixel size was 30 seconds and 42 μm , respectively. For the dry condition in Fig. 2 (a), it could be seen that the adsorber could be clearly visualized. Fig. 2 (b) was taken in an adsorption process after 8 minutes from the start. Adsorption amount was larger in the surface layer and around the fins and side walls (area A) due to the effective cooling, and was also larger in the area C around the thermocouples due to the larger porosity. On the other hand, adsorption amount in the bottom area of the bed (area B) was smaller. The reason might be due to the existence of inert gas.

On the other hand, in the desorption process, voids on the bottom wall due to a strong vapor generation by heating were observed just after the start (area D in Fig. (c), (i)). Then, the desorption progressed at a faster rate near the heat transfer surface (area E in Fig. (c), (i)).

Transient behaviors of adsorption amount distribution could be clearly observed by neutron radiography.

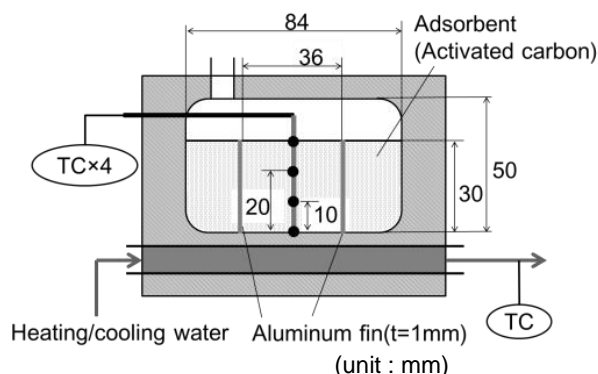
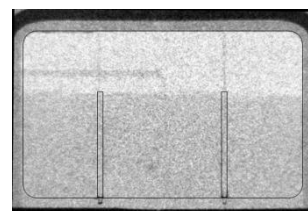
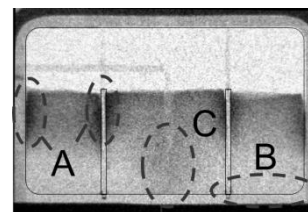


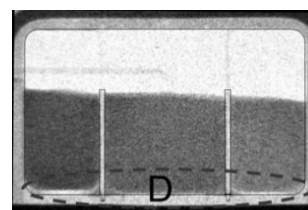
Fig. 1 Schematic of the tested adsorber.



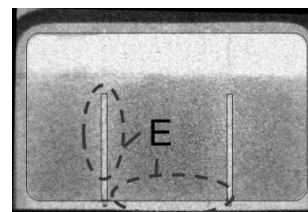
(a) Dry condition



(b) In adsorption process (after 8 min from the start)



(i) After 2 minutes from the start



(ii) After 120 minutes from the start

(c) Desorption process from the adsorption equilibrium.

Fig. 2 Visualized images by neutron radiography.
The darker part means higher adsorbed amount.

PR11-3 Neutron Radiography on Tubular Flow Reactor for Supercritical Hydrothermal Synthesis of Nanoparticles

T. Tsukada, K. Sugioka, K. Ozawa, S. Takami¹,
T. Adschiri², K. Sugimoto³, N. Takenaka³, Y. Saito⁴
and Y. Kawabata⁴

Dept. of Chemical Engineering, Tohoku University

¹*IMRAM, Tohoku University*

²*WPI-AIMR, Tohoku University*

³*Dept. of Mechanical Engineering, Kobe University*

⁴*Research Reactor Institute, Kyoto University*

INTRODUCTION: Recently, a variety of metal-oxide nanoparticles have been synthesized by supercritical hydrothermal synthesis [1]. For the design and optimization of the process, it is important to acquire the correct knowledge about the mixing behavior of cold aqueous feed solution and supercritical water in a hydrothermal reactor. Therefore, we used neutron radiography to visualize the flow in a tubular flow reactor for supercritical hydrothermal synthesis, and investigated the effects of the flow rates of two fluids and temperature of supercritical water on the mixing behavior in the reactor [2,3]. However, the obtained images were transmitted 2D images corresponding to the distributions of water density averaged along the direction of neutron. In this work, therefore, we have performed computed tomography (CT) using neutron beam to visualize the 3D distributions of water density in the reactor.

EXPERIMENTS: The experimental setup was similar to our previous works [2,3] except for using a rotating turntable for CT measurement. The tubular flow reactor had the T-junction comprised of Swagelok union tee and SUS316 tubes whose outer diameter and wall-thickness were 1/8 inch and 0.71 mm, respectively. Water at room temperature, corresponding to the feed aqueous solution, was mixed with supercritical water at the T-junction. In order to perform CT measurements, the T-junction was tightly fixed to a frame on the turntable, while smooth rotation of the T-junction was compensated by connecting with two high-pressure pumps through coiled 1/16-inch SUS tubes. During CT measurement, after one radiography image was taken, the turntable was rotated 0.90 degrees and the T-junction was exposed to 5 MW neutron beam for 60 s to obtain the next image. This sequence was repeated for 200 times while feeding and mixing supercritical water and room temperature water. Special care was taken to stabilize the whole system including the temperature of mixed flow before starting CT measurement. Being based on the images obtained, then, CT reconstruction of the images was carried out using Octopus software. In the experiment, pressure in the reactor was set to be 25 MPa.

RESULTS: Figure 1 (a) shows a vertical cross sectional image at the center of the T-junction. Here, supercritical water, which was fed from the top at temperature $T_{SC} = 375^{\circ}\text{C}$ and flow rate $Q_{SC} = 12$ g/min, was mixed with the room temperature water from the side (flow rate $Q_{RT} = 6$ g/min) at the mixing point. In this image, the darker area indicates the greater scattering of neutrons, i.e., the region where high-density, low-temperature water was flowing. After mixing, the room temperature water with high density flows along the side wall of the vertical tube. Fig. 1(b) shows the horizontal cross sectional images of the horizontal tube before the T-junction. From the figure, it is confirmed that a density-stratified layer, i.e., vertical distributions of water density, was generated in the horizontal tube owing to buoyancy. Also, Fig.1(c) shows the horizontal cross sectional images of the vertical tube after the T-junction. These images show that the room temperature water flows down along the side wall of vertical tube while the rest of region is filled with supercritical water. The two flows are gradually mixed after the T-junction. However, the density of water was not uniform at the last image in Fig. 1(c).

CONCLUSIONS: In this work, it was demonstrated that the CT using neutron beam allows us to visualize the 3D distributions of water density in a tubular flow reactor for supercritical hydrothermal synthesis of nanoparticles.

REFERENCES:

- [1] T. Adschiri *et al.*, *Green Chemistry*, **13** (2011) 1380.
- [2] S. Takami *et al.*, *J. Supercrit. Fluids*, **63** (2012) 46.
- [3] K. Sugioka *et al.*, *AIChE J.*, **60**, (2014) 1168.

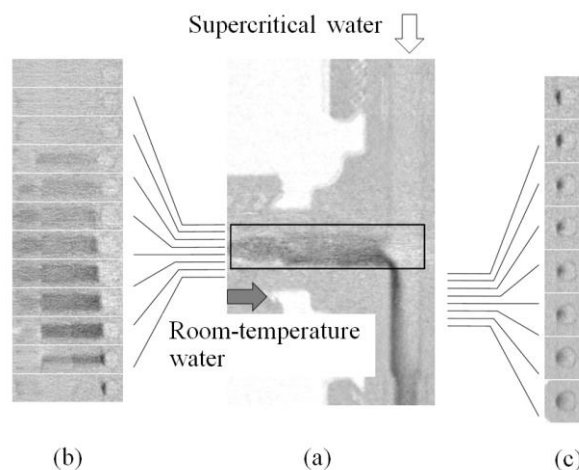


Fig. 1 3D images of mixing behavior in a tubular flow reactor using neutron CT.

H. Umekawa, T. Ami, S. Fujiyoshi, G. Yamashina,
R. Nakano, T. Harada, Y. Saito¹, D. Ito¹ and Y. Kawabata¹

Dept. Mech. Eng., Kansai University

¹Research Reactor Institute, Kyoto University

INTRODUCTION: In this series of the project, characteristics of the void fraction under several forced convective flow boiling conditions have been estimated so far. In this paper, the void fraction movement under oscillatory flow condition, especially, the influence of the heat capacity of the tube was introduced.

Although the most of the knowledge of the boiling flow has been obtained under steady flow condition, the unsteady flow, such as flow instability, strongly influences on the boiling characteristics. For example the CHF under oscillatory flow condition becomes less than half of the steady flow condition, and in these conditions the knowledge under steady flow condition is not enough to explain the phenomena. Moreover, these phenomena are influenced by the interaction between the wall temperature movement and flow structure, consequently the heat capacity of the tubes will be not able to be neglected.

EXPERIMENTS: In the experiment, the experimental apparatus was the forced convective boiling system of upward flow condition which could generate the artificial flow oscillation by using the mechanical flow oscillator. Thus the phenomena can be considered as the periodical phenomena which synchronized with the mechanical flow oscillator, and to obtain the high quantitatively dynamic image, the procedure of the ensemble average was able to be used [1]. The test sections were SUS 304 tubes, and the inner diameter of the test section was 5.0mm, heated length was 1000mm. In this case, two kinds of outer diameter tubes, i.e. 5.3mm and 11.0mm were used [2].

Figure 1 expresses the visualization images and the qualitatively measurement value of void fraction at several elevation position, pressure drop of test section, and orifice signal of the inlet flow rate. The dynamic images were obtained with enough quality as shown in Fig.1. Figure.2 is the comparison results of both tubes under same condition. As shown in Figures, the pressure drop of the thick wall tube expresses the calm characteristics than the thin wall tube case. On the other hand, in the thin tube case, the high void fraction period is much longer than that of the thick wall case. The total amount of the heat input of both cases were same value in electricity, but owing to the difference of the time response of the wall temperature, the instantaneous heat input amount may be slightly difference. The qualitatively measurement results show these differences clearly.

REFERENCES:

[1] H. Umekawa *et al.*, Physic. Procedia, **43** (2013) 269-276.

[2] S. Fujiyoshi, Master thesis of Kansai Unvi., 201.

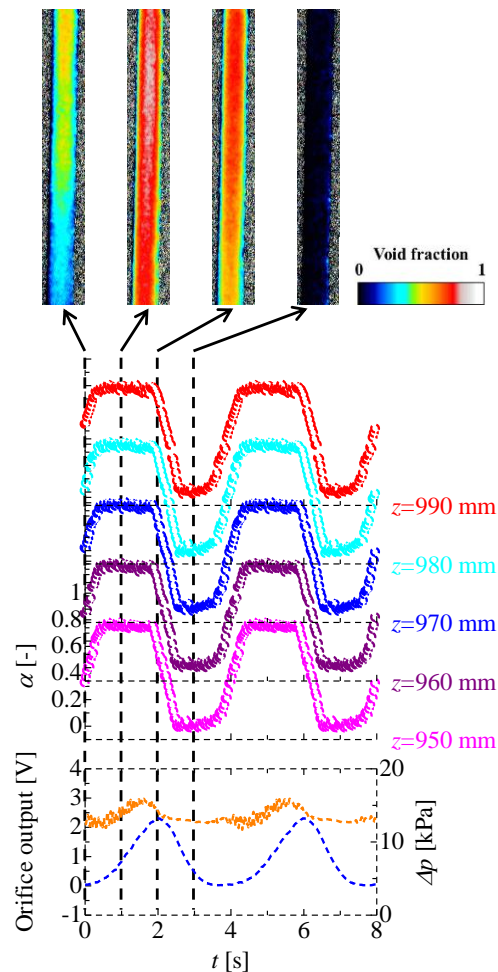


Fig.1 Results of O.D.=5.3mm tube. [2]

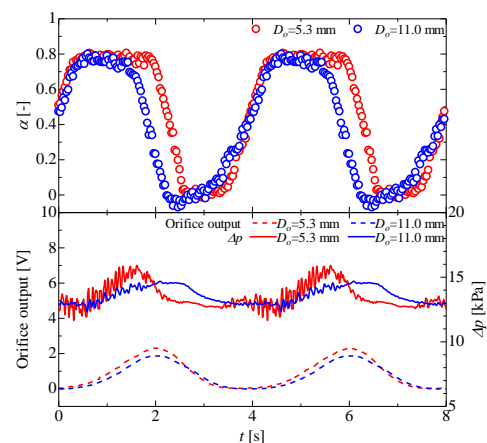


Fig.2 Comparison between O.D.=5.3mm and O.D.=11.0mm tubes. ($G_0=300\text{kg/m}^2\text{s}$, $\tau=4\text{s}$, $\Delta G/G_0=1.0$, $q=120\text{kW/m}^2$, $x_{\text{eq}}=0.00$) [2]

PR11-5 Neutron Imaging and Optics Development Using Simulation of VCAD Systems

Y. Yamagata, S. Morita, J. Guo, J. Kato¹, K. Hirota¹,
Y. Ohtake, H. Yokota, S. Wang, S. Mihara¹, H. Sunaga¹,
T. Sera², S. Sato³, Y. Kawabata⁴, Y. Saito⁴, M. Hino⁴,
M. Sugiyama⁴ and D. Ito⁴

RIKEN Center for Advanced Photonics, RIKEN

¹Nagoya University

²Osaka University

³KEK

⁴Research Reactor Institute, Kyoto University

INTRODUCTION:

VCAD System is a cluster of software codes, which can generate "real" object model in a computer and perform various numerical simulation. Those software codes include geometry conversion and input tools, 3D visualization, segmentation and mesh-generation tools, and various FEM-based simulation tools. The authors have been applied the neutron radiography data to VCAD systems to generate 3D geometry data and FEM analysis. Those software also include a simulation code for "real" optical components. Optical design and simulation software that are currently available deal with "ideal" optical surface without any profile error or scattering. V-Opt is a result of VCAD system research project utilizing discrete representation of Nagata patch. It can perform a ray tracing simulation with optical surfaces with profile errors and refractive index inhomogeneity. We have conducted neutron radiography experiments for 3D image reconstruction using VCAD system as well as neutron focusing mirror development.

EXPERIMENTS:

(1) Visualization of glue between steel plates

Bonding metallic material using glue is an important process for manufacturing motor cars, aircrafts and other industrial components. Since metallic materials are usually difficult to be penetrated by low-energy X-ray, it is almost impossible to visualize the distribution of a glue between steel plates. We tried to visualize the glue inside two steel plate by neutron radiography and subsequent CT reconstruction using KUR E-2 port. Two steel plates with dimension of 20mmx30mm t=3.0mm was glued by epoxy glue. 300 images are taken at E-2 port using neutron camera and reconstructed images are visualized and segment separated by using V-Cat software.

(2) Neutron Optics reflectometry test

To manufacture a neutron focusing mirror with relatively lower cost and manufacturing time, the authors have started the development of neutron focusing mirror using metallic substrate.[1] The advantage of metallic substrate are easier mechanical handling and shorter manufacturing time. A 50mm square test piece was fabricated with ultrahigh precision cutting with single crystal diamond tool and subsequent precision polishing. The reflectivity was measured at CN-3 port.

RESULTS:

Figure 1 shows the photo of the glued steel plates and the reconstructed image by neutron radiography. The non-uniform distribution of glue is clearly observed by neutron radiography, which may not be possible with X-ray imaging.

Figure 2 shows the 50mm square sample for metallic neutron focusing mirror. The substrate was stainless steel with amorphous nickel phosphate electroless plating. Thanks to the amorphous nature of NiP, the surface roughness was less than 1nm in average. 5 samples with different machining and coating condition was tested and diffuse scattering of the sample was evaluated. The roughness of metallic substrate was in acceptable level, but further improvement is desired.[2]

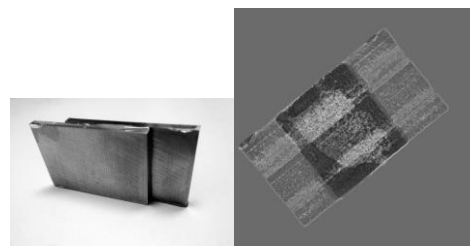


Fig.1 Reconstructed image of glued steel plates and a photo of original object

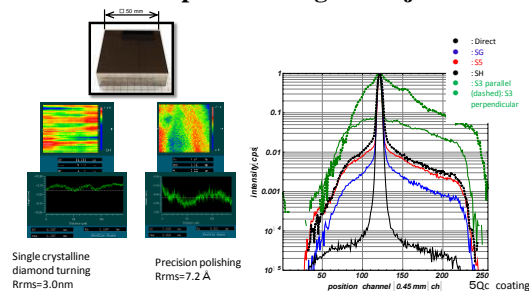


Fig.2 50mm metallic substrate sample for neutron focusing mirror and reflectivity measurement result (Direct: direct beam, SG: Reference glass substrate, S5: polished, S3: cut)

REFERENCES:

- [1] S. Takeda, H. Ohno, H. Sato, M. Furusaka, S. Morita, Y. Yamagata and M. Hino
International Workshop on Neutron Optics and Detectors, July (2013)
- [2] S. Takeda, J. Guo, S. Morita, H. Ono¹, T. Oda, J.Kato, H. Sato, M. Hino, Y. Yamagata and M. Furusaka
Union of Compact Accelerator-Driven Neutron Sources (UCANS IV), Sapporo, (2013)

採択課題番号 25P11-5 中性子ラジオグラフィによる工業製品の内部情報取得と プロジェクト
VCAD システムによるシミュレーション

(京大・原子炉) 齊藤泰司、川端祐司、杉山正明、日野正裕、伊藤大介

(理研) 山形豊、森田晋也、見原俊介、大竹淑恵、広田克也、横田秀夫、世良俊博、加藤純一、池上祐司

U. Matsushima, H. Shono, D. Ito¹ and Y. Saito¹

Faculty of Agriculture, Iwate University

¹Research Reactor Institute, Kyoto University

INTRODUCTION: Rice hulls can be a good plant growing medium for static solution culture without the need for aeration. Roots of the plants grown in the rice hull medium have two distinct functions: respiration at the upper part and uptake of water at the bottom part of the plant [1]. For static solution culture using the rice hull medium, we applied 2% sodium chloride (NaCl) solution to cultivate Komatsuna (*Brassica rapa* var. *perviridis* cv 'Misugi'). When this plant is placed in a medium containing such a high concentration of salt, usually, it withers and dies. We believe that a key to survive using high salt concentration solution is several different root functions appears in the rice hull medium. In this study, we investigated the changes in water and salt distribution in a root system in rice hull medium under static solution culture.

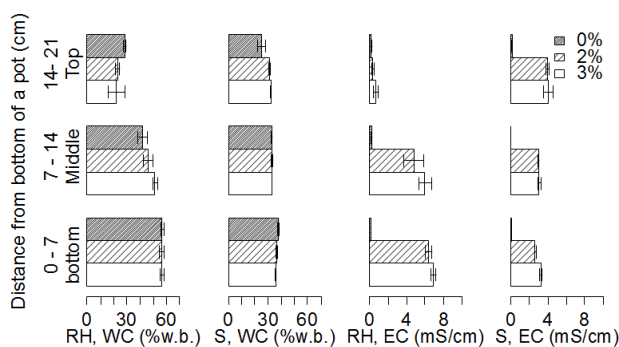
EXPERIMENTS: We performed neutron imaging according to the method described in our previous study [1] at the E2 hole of Kyoto University Reactor (KUR). We prepared 8 samples of the of Komatsuna plant according to the method described previously [1]. During the experiment, the plants were illuminated using 4 halogen lamps to induce photosynthesis. The sample plant was not watered for 24 h. During this dry period, 2 neutron images were captured. Then, the samples were divided into two treatment groups and immersed in 5-cm depth of two different solutions, 2% NaCl solution and water. During this wet period, we captured an additional 9 neutron images.

In addition, we performed a cultivation experiment in a greenhouse at Iwate University. Rice hull medium and soil samples from an Iwate University experimental farm were used to grow Komatsuna. We planted 3 plant samples in a pot (diameter, 10 cm and height 25 cm) containing medium up to 22 cm. The pots were placed in three different solutions at a depth of 1 cm; the solutions were water and 2% and 3% NaCl. After cultivation, root growth on the surface of the medium was photographed. The medium was divided into 3 layers (top, middle, and bottom), and then, we measured the water content and electrical conductivity (EC).

RESULTS: During the dry period, all samples were healthy and fresh. After initiation of the wet period, the samples immersed in the 3% NaCl solution gradually wilted. The salt solution induced an initial reaction of

water stress in plants. To compare the role of root function among different treatments, the samples should adapt to the treatment conditions in advance. For the subsequent experiment, 2% NaCl solution should be applied at least one week before the experiment.

At the first phase of this cultivation experiment, Komatsuna samples that were immersed in 2% and 3% NaCl solution showed an initial salt stress reaction similar to that observed in the experiment performed at KUR. However, the samples gradually adapted to the salt solution. Although the samples were immersed in the salt solution, the root system was well developed at the surface of the rice hull medium. On the other hand, the root system on the soil surface was thin when it was immersed in the salt solution. Water content of the soil was consistent in the bottom and top layers (Fig. 1). EC of the soil was the highest in the top layer. We observed salt accumulation at the soil surface similar to that usually seen at salt-damaged farms. On the other hand, water content of the rice hull decreased with an increase in the height of the medium. EC in the rice hull medium immersed in salt solution showed similar decrease to that of water content. The absence of salt accumulation in rice hull medium facilitated the development of root system. Capillary pressure easily raises a solution depending of the particle size of the medium. Therefore, capillary pressure of the soil is higher than that of the rice hull medium because of the smaller particle size of soil. The salt solution reached the soil surface, and dehydration of water from the surface resulted in accumulation of salt in the top layer. Less capillary pressure of the rice hull medium created gradients of water content and salt concentration. Because of the concentration gradient, certain areas of the root system may adapt to the salt concentration in



the rice hull medium.

Fig. 1. Water content (WC) and electrical conductivity (EC) of rice hull medium (RH) and Soil (S).

REFERENCES:

[1] U. Matsushima *et al.*, KURRI progress Report 2012, (2012) 128.

PR11-7 Measurement of Water Content in Hardened Cement Paste by Neutron Imaging

T. Numao, T. Harada, T. Kimura, T. Abe,
K. Watanabe¹, Y. Ohno¹, Y. Kawabata² and Y. Saito²

Department of Engineering, Ibaraki University

¹Railway Technical Research Institute

²Research Reactor Institute, Kyoto University

INTRODUCTION: Hardened cement paste shrinks with drying or swells with wetting. This repeated shrinking and swelling of the paste affects the paste's long-term durability. Therefore, it is important to characterize the moisture distribution inside hardened cement paste and the deformation associated with moisture movement.

In this study, the experiments were carried out to investigate the relationship between the beam-hardening effect and the intensity of neutron beam penetrating water as part of the studies to quantify the moisture content in hardened cement paste by using neutron radiography. The authors developed a correction formula and adjusted the formula for each test result to identify the moisture volume by using the penetration distance.

EXPERIMENTS: In this study, ceramic specimens made of aluminum were used instead of hardened cement paste because of taking no account of the hydration of cement. Fig.1 shows the test specimens which were cylindrical aluminum container (13 mm in diameter and 10 mm high) and columnar ceramic made of sintered alumina (Al_2O_3) (about 13 mm in diameter and about 10 mm high) to contain certain percentages of water content. The number after the alphabet shows the percentage of water content.

Figure2 shows representative neutron radiographic images. Fig.3 shows the relationship between $-\ln(U')$ and the $\mu\sigma$ value of water. The experimental values was smaller than the theoretical value ($\mu = 0.347$) and decreased with increasing penetration distance. This phenomenon is the beam-hardening effect. The authors developed a correction formula (2) on the assumption that $\mu\sigma$ can be expressed by an exponential function.

$$I = I_0 \exp(-\mu\sigma) \quad (1)$$

$$U'' = \exp(U') \times \alpha = \mu\sigma \quad \alpha = 0.6 \quad (2)$$

RESULTS: These results suggest that the beam-hardening effect can be corrected. However, the coefficient developed in this experiment is applicable only to the images taken under the conditions of this test. It is necessary to develop a coefficient that can be used for capturing images under various conditions.

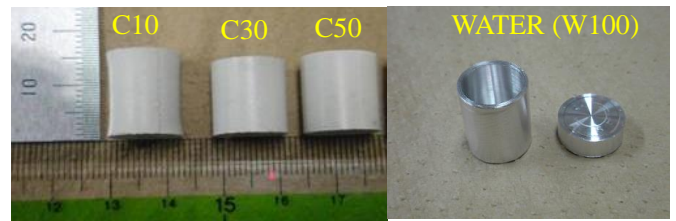


Fig. 1. Test Specimens

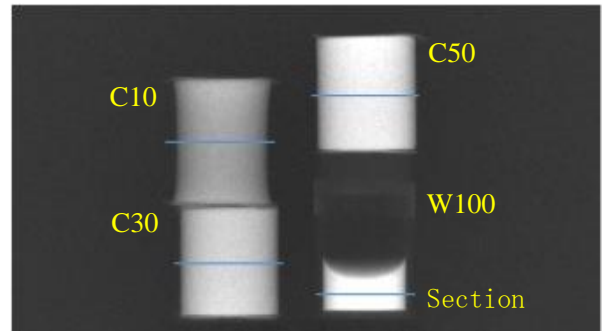


Fig. 2. Neutron radiographic images

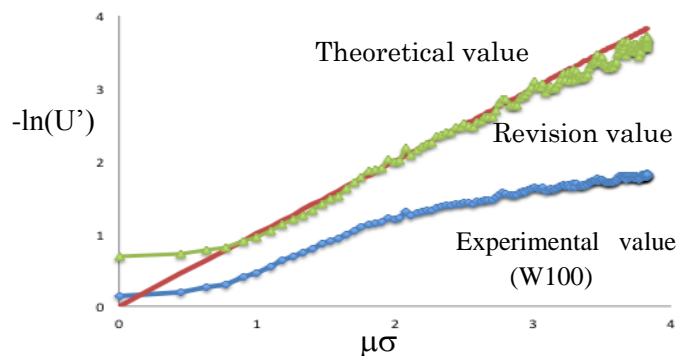


Fig. 3. Relationship between $-\ln(U')$ and the $\mu\sigma$ value of water.

REFERENCES:

- [1] I. Funakawa, T. Numao and H. Iikura
Journal of Japan Society of Civil Engineers, Ser. E2
Vol. 67(2011) 596–604.
- [2] T. Numao *et al.*,
67th Annual Academic Lecture of Japan Society of Civil Engineers, V-040(2012)

H. Kagawa, T. Nagata, T. Masuoka, H. Ikeda, D. Ito¹,
Y. Saito¹ and Y. Kawabata¹

Propulsion Group, Japan Aerospace Exploration Agency
²Research Reactor Institute, Kyoto University

INTRODUCTION: Neutron radiography can reveal invisible objects such as fluids like X-ray technology. We tried to apply this technology to observe a thruster, which is one of the key sub-components for spacecraft using fluids as propellants. Last year, we directly observed the physical and chemical phenomena occurring within the catalyst bed of the mono-propellant thruster using neutron radiography at the Kyoto University Research Reactor, but lacked any reference to understand quantitatively the dynamic behavior of the hydrazine acquired by neutron radiography. Thus, the purpose of this study is to estimate the macroscopic of the hydrazine for thermal neutrons and then analyze the dynamic behavior of the injected hydrazine quantitatively.

EXPERIMENTS: We prepared the same equipment as used last year, which involved installing two mono-propellant thrusters to the portable test equipment in parallel, as shown in Fig. 1.

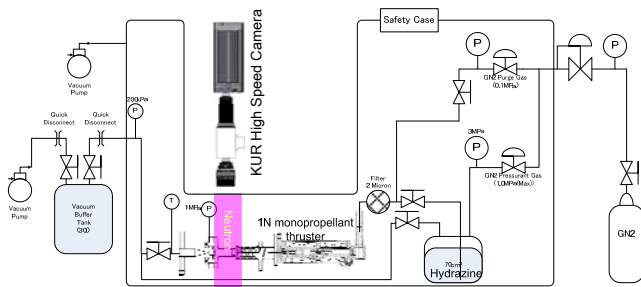


Fig. 1 Schematic of the visualization equipment

We also prepared a calibration cell for neutron transmission as shown in Fig.2. The inner gap of the calibration cell changes from 0.2mm to 2mm, which enable to measure the variation of the image brightness with the hydrazine thickness.

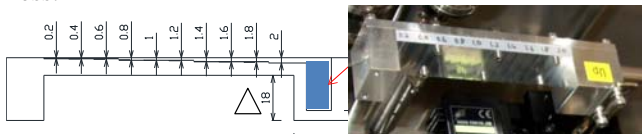


Fig. 2 Calibration cell for neutron transmission in hydrazine layer.

The calibration cell was installed between the high-speed image-acquisition system and the KUR B-4 imaging port, while the cells were sliding horizontally in 0.2mm steps to vary the gap thickness from 0.2 to 2.0 mm.

RESULTS: The calibration images and the averaged brightness were shown in Fig. 3. The variation of the logarithm of the obtained image brightness with the thickness show good similarity and linearity, from which the macroscopic cross section of the hydrazine can be easily calculated.

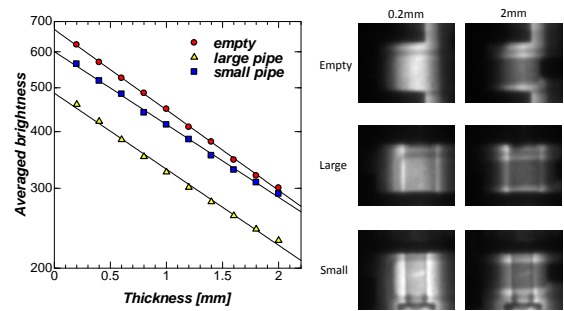


Fig. 3 Variation of the brightness and the original images.

The temporal fluctuations of the image brightness at three areas of the thruster images were shown in Fig. 4. The image brightness at the upper area decreased when the hydrazine was injected into the thruster catalyst bed. The image brightness at the bottom and middle areas did not decrease like the bottom area. Such brightness fluctuations show how the phase change of hydrazine takes place in the upper area. In addition, the hydrazine thickness at the area was calculated from image brightness by taking the macroscopic cross section into account.

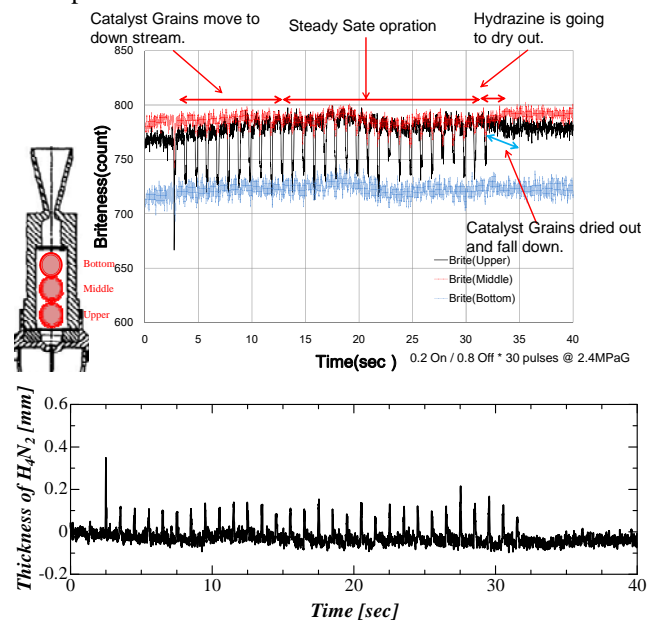


Fig. 4 Temporal fluctuations of brightness and hydrazine thick-ness.

CONCLUSIONS: Shooting of neutrons at KUR was conducted using a real hydrazine propellant thickness indicator. The macroscopic cross section of the hydrazine was estimated by calibration experiments and was applied to the successive neutron images to estimate the hydrazine distributions. The results and technologies will help JAXA efforts to extend the lifespan and reliability of thrusters.

REFERENCES:

- [1] H. Kagawa and D. Ito *et al.*,
10th International Symposium on Special Topics in
Chemical Propulsion & Energetic Materials, 2014

H. Iikura, T. Sakai, R. Yasuda, T. Nojima,
M. Matsubayashi, Y. Saito¹, D. Ito¹ and Y. Kawabata¹

Quantum Beam Science Directorate, Japan Atomic Energy Agency
¹Research Reactor Institute, Kyoto University

INTRODUCTION: We developed a new simple technique for increasing light intensity from a neutron scintillator using brightness enhancement films (BEFs) [1]. This technique can be applied to neutron imaging only by attaching the BEFs on the output surface of the scintillator. Our previous research showed that this technique can enhance the light intensity by 2.5~2.8 times using 65µm thick BEFs. In this study, the influence of the thickness and prism pitch of BEFs on the brightness and spatial resolution of a neutron imaging system were investigated using several different types of BEFs.

EXPERIMENTS: Neutron imaging was carried out at the neutron radiography facility (E-2 beam hole) installed in KURRI. The camera system consists of a BU-53LN cooled charge coupled device camera (BITRAN) and an 85 mm lens (Nikon Nikkor, F = 1.4) with extension rings (Nikon). Figure 1 shows the schematic configuration of the imaging system installed to the E2 beam hole. In this study, a commercial type scintillator called NR-converter (Kasei Optonix) was used as the neutron converter. The light converted by the NR converter is reflected once by a single mirror to be transported to the camera system. This C-CCD camera has 4008×2672 pixels and provides 16 bit digitization. Because the view size using this 85 mm lens is about 150×100 mm², the pixel size becomes approximately 40×40 µm².

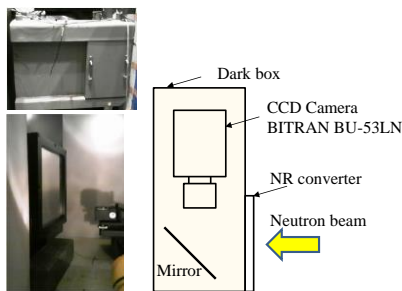


Fig. 1 Schematic view of the imaging system.

Figure 2 shows a schematic of the BEF consisting prismatic structures and a polyester substrate. For enhancing the light intensity from the scintillator, two BEFs were stacked perpendicularly and placed on the NR converter, and silica glass was pressed on the films in order to stick to the converter as shown in Fig. 3.

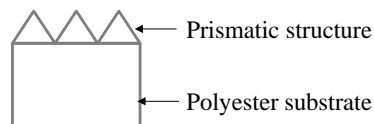


Fig. 2 Schematic of BEF.

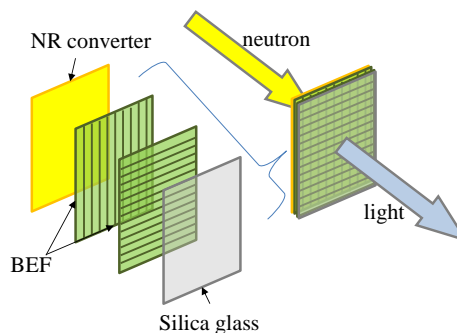


Fig. 3 Setup of BEF to NR converter.

RESULTS: Two kinds of BEFs were tested in this study. One has 65µm thickness and the other 45µm. Experimental results show that the thickness of the BEFs does not affect the light intensity at present experimental conditions. In addition, the spatial resolution was not modified by using the thinner BEF (45µm), which may be attributed to the imperfect setup. Thus, further investigation should be carried out.

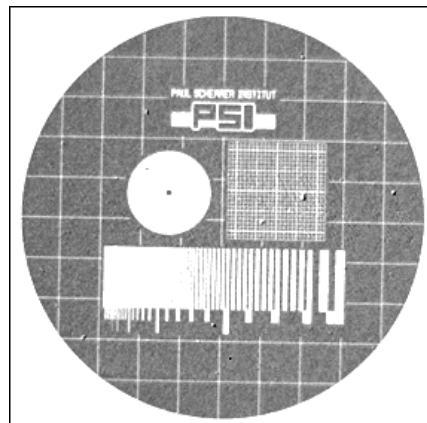


Fig. 4 Neutron image of PSI indicator using BEF.

REFERENCES:

[1] H Iikura *et al.*, Physics Procedia, **43** (2013) 161-168.

PR11-10 In-situ Neutron Radiography Investigation on the Hydraulic Behavior of High Strength Cement Paste under High Temperature

M. Kanematsu, R.Inose, M. Nakano, M. Tamura¹,
N. Tuchiya², Y. Saito³ and Y. Kawabata³

Tokyo University of Science

¹The University of Tokyo

²Building Research Institute

³Research Reactor Institute, Kyoto University

INTRODUCTION: High strength concrete (HSC) subjected to high temperature heating tends to show explosive spalling due to low permeability of cement paste matrix. The dense cement paste of HSC prevents heated water from escaping, resulting in forming a high pore pressure. Furthermore, dehydration of cement paste, such as calcium silicate hydrate (CSH) and calcium hydroxide (CH), under high temperature could possibly affect to the explosive behavior of HSC. However, the detailed mechanism of the explosive spalling behavior of HSC has not been fully understood. To increase the understanding of the spalling mechanism of HSC, high strength cement paste (HSCP) was used to focus on the water behavior in the paste of HSC under high temperature. Neutron radiography (NR) was applied to visualize and to quantify the in-situ water behavior in HSCP under high temperatures.

EXPERIMENTS: HSCP (100x100x20mm³) heating experiment was conducted in TNRF and temperature of each location in the specimen was measured by using thermocouple-type thermometer. The temperature at the bottom surface of the specimen was controlled by the flame of Bunsen burner with mass flow controller. Neutron radiography measurement was performed at Kyoto University Research Reactor Institute. Neutron flux and resolution of image is $1 \times 10^7 \text{ n/cm}^2$ (1MeV) and $100 \mu\text{m/pixel}$, respectively. Imaging interval including operation time was 5.5 sec/image. To estimate the amount of water due to dehydration process of hydration products formed in the sample quantitatively, TG/DTA analysis was carried

RESULTS AND DISCUSSION: The correlation of

change in water and the intensity of transmitted neutron were determined using specimen with predetermined specific water contents. Differential intensity per unit volume paste was calculated from the transmission images as shown in Fig. 1 and distribution of water content per unit volume paste are shown in Fig. 2. Over saturated area which contain comparatively higher amount of water content presented as liquefied phase were confirmed in the region of around 100°C. This water condensation area could be pushed up to the top with elevation of temperature. Also over dried area was observed in the specimen, it is assumed that the dehydration of hydration products in the paste enhances the increase of the amount of water in this area. According to the TGA results, the mass loss in the range of 120 to 350°C and 350 to 550°C are attributed to the decomposition of CSH and CH, respectively. From increase of mass loss at 120-350°C depending on the distance from heating surface, dehydration of CSH could be assumed to be the one possible reason of the formation of the water saturated region.

CONCLUSION: In the present study, the drying process in the HSCP by heating was clearly visualized and quantified using in situ NR. Presence of zones in the HSCP containing comparatively high liquid phase water contents was also observed around the region at 100°C. Based on TG-DTA analysis, it is found that condensed water and water occurring due to the dehydration of CSH affect the formation of this water saturated region.

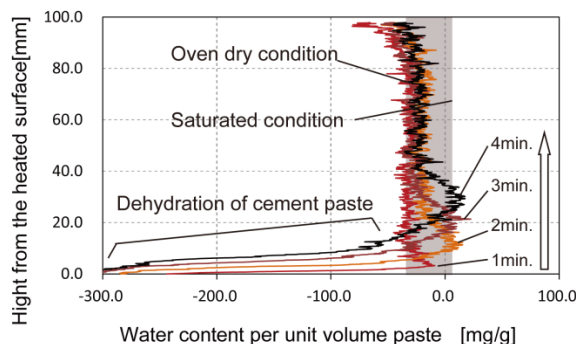


Fig.2 Distribution of water content per unit volume paste

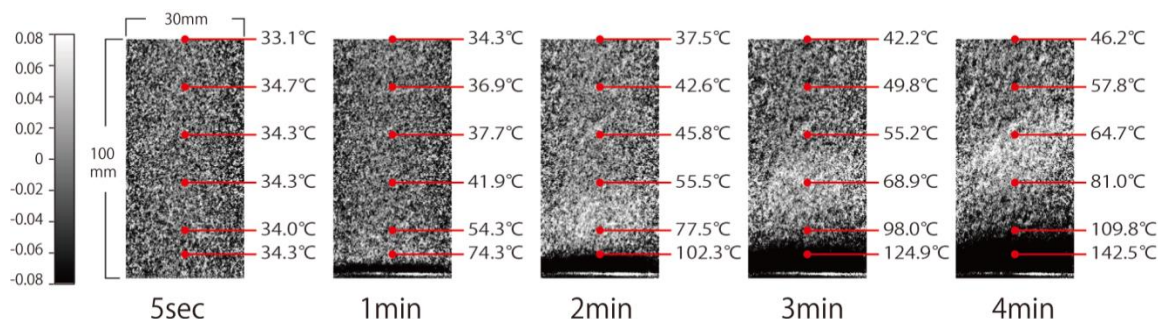


Fig.1 Differential water content of cement paste

K. Mizuta, Y. Saito¹ and D. Ito¹

Faculty of Engineering, Kagoshima University

¹ Research Reactor Institute, Kyoto University

INTRODUCTION: Thermal management in electronic devices is getting more serious, because the lack in cooling capability in such devices causes various reliability problems and decreases their working efficiency. In particular, such poor cooling capability in a LED array leads to poor quality of lighting. Because the light emitting efficiency of the LED array decreases with increasing working temperature, such poor cooling capability of the LED array causes its reliability problems and also non-uniform profile of the light emitting efficiency. To solve such thermal management problems, a flat heat pipe such as vapor chamber is one of the attractive solutions for its higher effective thermal conductivity than that of metal materials [1]. In conventional flat heat pipes, however, their heat transfer characteristics are strongly affected by installation posture, because the coolant distribution inside flat heat pipe is strongly affected by gravity. Recently, a novel flat heat pipe called FGHP (Fine Grid Heat Pipe) was developed by Morex Kiire Co., Ltd. located in Kagoshima. In the previous study, we found that the heat transfer characteristics of the FGHP are scarcely affected by its installation posture. In this study, we have evaluated the distribution of coolant in FGHP heat spreader utilizing neutron radiography in Kyoto University Research Reactor Institute in Japan to clarify the postural effect on heat transfer characteristics of FGHP heat spreader.

EXPERIMENTS: Experiment was conducted in the E-2 port in KURRI. The size of the test sample of FGHP heat spreader was 65 mm square and 2 mm thick. The face of the test sample was set vertically. A ceramic heater attached at the center of the heat spreader was used for heating, and three pin-fin type aluminum heat sinks attached opposite side were used for cooling. Neutron radiography images were captured under various heating conditions. CA type thermocouples were utilized to measure surface temperature of the heat spreader and atmospheric temperature, with which the thermal resistance of the FGHP was calculated. To evaluate the effect of gravity on coolant distribution, the intensity of penetrated neutron beam at four different positions in the test sample was calculated from neutron radiography images. Temporal variation of the intensity was normalized by that at the particular point outside of the sample. The change in coolant distribution with heat input was evaluated by normalized intensity calculated by the following equation:

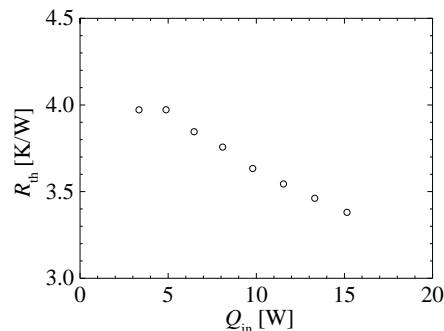


Fig. 1. Variation of thermal resistance with heat input.

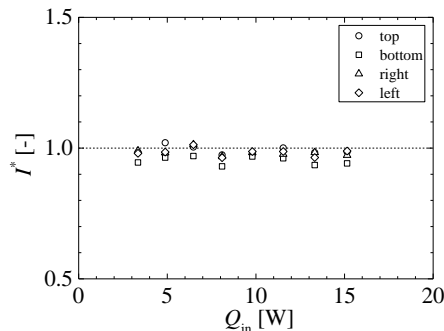


Fig. 2. Variation of I^* with heat input.

$$I^*(x, y) = \frac{I(x, y)}{I_0(x, y)}, \quad (1)$$

where, $I(x, y)$ and $I_0(x, y)$ are values of intensity obtained under heating and adiabatic conditions, respectively.

RESULTS: Figure 1 shows the variation of thermal resistance with heat input. As shown in Fig. 1, thermal resistance begins to decrease with increasing heat input, which resulted from the coupled effect of increase in heat transfer coefficient and increase in effective thermal conductivity of FGHP as observed in the previous study. Figure 2 shows the variation of normalized intensity with heat input. As shown in Fig. 2, the intensities at top, right and left show similar tendency under heating and adiabatic conditions, though the intensities at the bottom position are a little smaller under heat conditions. The intensities are nearly constant regardless of the heat input at all measured points. These measurement results indicate that uniform coolant distribution in FGHP can be realized regardless of the heat input and installation posture, which may lead the uniform heat spreading performance of FGHP under its operating conditions.

REFERENCES:

- [1] J. C. Wang, Int. J. Heat Mass Transf., **53** (2010) pp. 3990-4001.